



Melting behavior and structural and morphological changes of isotactic polypropylene from heat treatment

Katsuharu Tagashira¹ · Masanori Maruyama¹ · Yoko Mizutani¹ · Hiroshi Kajioka¹ · Kazuhiko Sakai¹ · Kiyoka N. Okada² · Masamichi Hikosaka²

Received: 20 July 2018 / Accepted: 2 October 2018 / Published online: 9 November 2018
© The Society of Polymer Science, Japan 2018

Abstract

Time-resolved X-ray measurements during melting and detailed structural and morphological analyses of samples heat treated near their melting temperature for a short time revealed a structural change of isotactic polypropylene (iPP) in which the melt-crystallized at a cooling rate (CR) of 20 K/min. During melting at a heating rate (HR) of 5 K/min, we observed the appearance of a peak with a higher melting temperature (T_m); however, we could not clearly observe -231 , -161 reflections that are typical for an $\alpha 2$ crystal. The $\alpha 2$ crystal was a minor component of the heat-treated sample with elevated T_m in which reorganization was almost completed during the heat treatment. These results suggest that lamellar thickening of the $\alpha 1$ crystal is the main mechanism of reorganization. Lamellar thickening was accompanied by an increase in central diffuse scattering of small-angle X-ray scattering (SAXS), suggesting that thickening occurred at randomly distributed positions and resulted in the disordering of lamellar stacking observed based on observations with a transmission electron microscope (TEM) for the heat-treated samples. The drastically increased long period (L) above 160 °C, which can be attributed to the partial melting of thin lamellae, was maintained after the heat treatments by the aforementioned reorganization.

Introduction

Since the structure of the crystalline polymer material obtained using the usual processing method is in a metastable state, it changes into a stable structure through heating. Therefore, it is important to elucidate this structural change because it leads to improvement of material performance.

Isotactic polypropylene (iPP) is a crystalline polymer that is inexpensive, lightweight (specific gravity of approximately 0.90), has a high melting point (approximately 160 °C), is easy to mold, and hence is widely used in automotive parts, home electric appliances, food packaging films, etc. iPP is also environmentally friendly, highly recyclable, and does not generate toxic gases even when it is burned; therefore, replacement with other resins such as engineering plastics and other ordinary resins is proceeding. As a result, 2.5 million tons are demanded in Japan and approximately 50 million tons are demanded in the world per year.

In studies of the melting behavior of iPP, the dependence on the heating rate (HR) of multiple melting behaviors measured by a differential scanning calorimeter (DSC) is commonly reported [1]. In the DSC, iPP crystallizes at 130 °C or lower temperatures from a molten state, and an endothermic peak or a shoulder appears on the high-temperature side of a primary melting peak when the HR is 2 K/min or less [1, 2]. The increase in melting point due to thickening of lamellar crystals is more prominent at a lower HR [2].

With regard to the structural change in iPP, a study of the conversion of an $\alpha 1$ crystal by heat treatment (158–162 °C for 5 min) into the most stable $\alpha 2$ crystal has been reported [3]. The arrangement of CH–CH₃ bonds (upward or downward) in the unit cell shows complete order in an $\alpha 2$ crystal, whereas it does not in an $\alpha 1$ crystal. The ordering of the upward and downward arrangement of adjacent polypropylene chains in the unit cell of iPP is disordered in an

✉ Katsuharu Tagashira
Katsuharu_Tagashira@sunallomer.co.jp

² Graduate School of Integrated Arts and Sciences, Hiroshima University, Hiroshima, Japan

¹ R&D Division, SunAllomer Ltd, Kawasaki, Japan

$\alpha 1$ crystal but is regular in an $\alpha 2$ crystal [4]. For the identification of an $\alpha 2$ crystal, reflections in which $h + k$ equals an odd number such as -231 , -161 in wide-angle X-ray diffraction (WAXD) are used [4], where h and k are Miller indices. Reflections in which $h + k$ equals an even number are common for $\alpha 1$ and $\alpha 2$ crystals. A simple measure of the ratio of an $\alpha 2$ crystal ($M_{\alpha 2}$) to the total crystal is calculated by the ratio $I(\alpha 2)/I(\alpha 1 + \alpha 2)$. $I(\alpha 2)$ is the intensity of the reflection that is unique to the $\alpha 2$ crystal, while $I(\alpha 1 + \alpha 2)$ is the combined intensity of the 071 and 161 reflections that are unique to the $\alpha 2$ crystal and the -241 , 221 reflections that are common to $\alpha 1$ and $\alpha 2$ crystals observed in the same position [5]

With regard to the morphological change, iPP characterized by a bamboo leaf-like or needle-like morphology with a melting temperature (T_m) near the equilibrium melting temperature (T_m^0) was obtained by heating and annealing a prequenched mesophase sample at a selected HR and at an annealing temperature of 166 °C for 24 h [6]

However, the type of structural and morphological change that accompanies melting and heat treatment is not clear. The purpose of this report is to elucidate the structural and morphological changes that occur during melting and heat treatment near the melting temperature (160 °C, pretreatment of 155 °C for 1 min and 160 °C) for a short time (total 4 min) by means of an X-ray scattering method and to clarify the mechanism of reorganization in an iPP crystal. This clarification of the relationship between crystal structure and morphology is meaningful to the understanding of the structural formation of crystalline polymers.

Experimental section

Sample

The iPP ($M_w = 298,000$, $M_w/M_n = 7.1$, $m_{\text{mmm}} = 97.2\%$) was produced by SunAllomer Ltd, where M_w is the weight-averaged molecular weight and M_w/M_n is the molecular weight distribution measured by GPC, and m_{mmm} is a meso-pentad value measured by ^{13}C -NMR, a measure of isotacticity. The equilibrium melting temperature (T_m^0) was estimated as 182 °C considering the molecular weight [7] and the isotacticity [8]. A 6–7 mg disk was cut from a sheet (thickness: 0.3 mm) of the iPP obtained by the casting process. The iPP disk was melted at 230 °C for 5 min in a DSC pan and was crystallized at a cooling rate (CR) = 20 K/min to 30 °C. It was then used as a starting sample (denoted as “230C5m”) for the observation of structural change during melting and heat treatments.

Heat treatment and observation of the melting and crystallization behavior by DSC

Heat treatment and observation of the melting and crystallization behavior were performed using a Perkin-Elmer Diamond DSC under a nitrogen flow of 0.15 MPa.

Observation of structural change during melting by time-resolved X-ray measurement

After the melt-crystallized sample was removed from the DSC pan, it was wrapped in a Kapton membrane to prevent the sample from flowing at high temperature and was set in a heating stage (LINKAM THMS 600). Time-resolved WAXD/SAXS (small-angle X-ray scattering) measurement was performed during melting at the prescribed HR at SPring-8, BL 03 XU, 2nd hatch. The X-rays (wavelength: 0.1 nm, beam size: 100 $\mu\text{m} \times 120 \mu\text{m}$) were incident on the sample surface in the vertical direction (Through). The camera length was 254 mm for WAXD and 1850 mm for SAXS. The exposure time of one measurement was 2 s for WAXD at a high angle ($2\theta = 17\text{--}35^\circ$) to examine the existence of $\alpha 2$ crystals, and 1 s using a Mo 40 μm filter for WAXD at a low angle ($2\theta = 4\text{--}16^\circ$) to determine crystallinity, where 2θ is the scattering angle. The exposure time of one measurement was 0.1 s for SAXS. Considering the sample damage that occurs due to synchrotron radiation, the measurement interval was adjusted so that total irradiation time of a sample was maintained at 180 s for different HRs.

The circle ring average of the two-dimensional (2D) WAXD profile detected by the Flat Panel Display was obtained in the range of $\beta = 0\text{--}20^\circ$ for the low-angle region and $\beta = 0\text{--}60^\circ$ for the high-angle region, where β is the azimuthal angle. The circular ring average of the 2D SAXS profile detected by the II + CCD was made across the entire range of q , where q is the scattering vector. After the circle ring average, the background was corrected to obtain the scattering intensity ($I_{\text{WAXD}}(2\theta)$ and $I_{\text{SAXS}}(q)$). The index of crystallinity ($\chi_{\text{c, WAXD}}$) was obtained by separating the I_{WAXD} profile in the range of $2\theta = 7.9^\circ\text{--}15.1^\circ$ into an amorphous component and a crystalline component. The calculation was made using a simplified method based on the Hermans–Weidinger method [9] (Eq. (1)),

$$\chi_{\text{c, WAXD}}(\%) = (S_{110} + S_{040} + S_{130} + S_{111} + S_{-131,041})/S_{\text{all}} \times 100, \quad (1)$$

where S_{hkl} is the integrated intensity of the hkl reflection and S_{all} is the total integrated intensity in the mentioned range. The long period (L) was obtained by $L = 2\pi/q_{\text{peak}}$, where q_{peak} is the peak position of I_{SAXS} after the Lorentz

correction ($q^2 \times I_{\text{SAXS}}$) [10]. The Lorentz correction was applied to the scattering that originated from periodically aligned lamellae and was not applied to central diffuse scattering [11].

Observation of the structure of heat-treated samples by X-ray measurement

WAXD measurements were performed using a Rigaku RINT-RAPID with an imaging plate (IP) as a detector at room temperature. The X-rays (wavelength: 0.154 nm, beam size: $800 \mu\text{m} \phi$) were incident on the sample surface in the vertical direction (Through), and the camera length was 191 mm. We confirmed that no preferred crystal orientation existed in the samples by checking the change in intensity of the 110 and 040 reflections in the β -scan. After circle ring averaging of the obtained 2D profile, the background was corrected to obtain $I_{\text{WAXD}}(2\theta)$. The index of crystallinity ($\chi_{\text{c, WAXD}}$) and the measure of the ratio of the $\alpha 2$ crystal ($M_{\alpha 2}$) were obtained using the methods described above. For the calculation of $\chi_{\text{c, WAXD}}$, the range of 2θ was adjusted in order to use the same range of q .

SAXS measurements were performed at SPring-8, BL 03 XU, 2nd hatch at room temperature. The X-rays (wavelength: 0.15 nm, beam size: $30\text{--}40 \mu\text{m} \phi$) were incident on the sample surface in the vertical direction (Through), and the camera length was 3247 mm. The circular ring average of the 2D scattering profile detected by IP was made across the entire range of q . After the circle ring average, the background was corrected to obtain $I_{\text{SAXS}}(q)$. A Lorentz correction ($q^2 \times I_{\text{SAXS}}$) was applied to the scattering that originated from periodically aligned lamellae but was not applied to central diffuse scattering as mentioned above.

Observation of the morphology of heat-treated samples by optical microscopy and transmission electron microscope

The morphology of spherulites was observed from a thin section that was cut from the sample that was removed from the DSC pan by using a polarized optical microscope (OLYMPUS BX51) with a quarter-wave plate, U-TP530.

For transmission electron microscope (TEM) observation, a sample that was cut from the disk that was removed from the DSC pan was immersed in a 0.5% RuO_4 aqueous solution overnight after the surface of the sample was smoothed with a cryomicrotome. After staining, ultrathin-sections approximately 100 nm thick were obtained with the cryomicrotome by cutting at -100°C . The resulting ultrathin-sections were collected on a mesh with a collodion membrane and were used as specimens for TEM observations. TEM observations were conducted using a HITACHI HF-2200 with a CCD camera, Gatan Orius 600SC at

200 kV of accelerating voltage. Image analysis of the photographs was performed using the software Image-Pro Plus 5.1J to obtain the lamellar thickness and its distribution. The border between each lamella and an amorphous region or other lamellae was made by visual judgment. For each lamella, thicknesses were measured at 2 to 5 points and their average value (l_c) was calculated. From l_c and the length, which was also measured, the area of each lamella was calculated and a histogram showing the relation between the fraction of the area of each lamellae ($f(l_c)$) and l_c was prepared. The average lamellar thickness ($\langle l_c \rangle$) was calculated by integrating the product of each l_c and $f(l_c)$.

Results

Structural change during melting with different HRs

Figure 1 shows the DSC curves during melting of the sample that was crystallized from the molten state at a CR of 20 K/min for HR = 5 and 20 K/min. We found that the melting curve showed a single endothermic peak ($T_m = 162^\circ\text{C}$) when the temperature was rapidly raised at HR = 20 K/min and that it showed double endothermic peaks ($T_m = 161$ and 168°C) when the temperature was slowly raised at HR = 5 K/min (where T is the temperature).

Figure 2 shows the change in the WAXD profiles when the temperature was increased with HR = 5 and 20 K/min. In the both cases, the reflections of -161 and -231 near $2\theta = 19.5^\circ$, which are normally used for the identification of the $\alpha 2$ crystal [4], were not clear. Figure 3 shows the temperature dependencies of $\chi_{\text{c, WAXD}}$ for HR = 5 and 20 K/min. $\chi_{\text{c, WAXD}}$ showed higher values for a low HR of 5 K/min than for a high HR of 20 K/min when T is higher than 150°C .

Figure 4 shows the SAXS profiles for HR = 5 and 20 K/min. In the comparison of SAXS profiles with

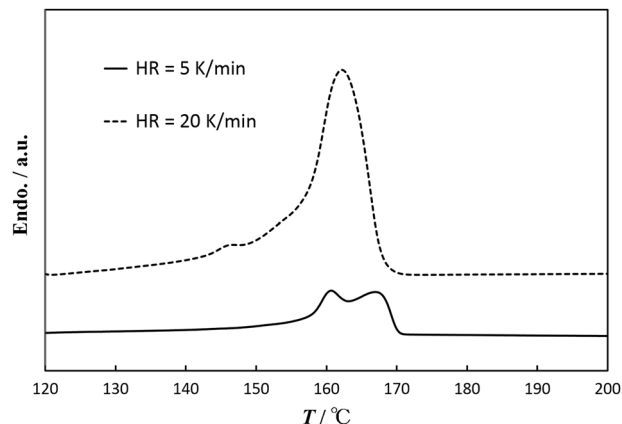


Fig. 1 DSC profiles for HR = 5 and 20 K/min

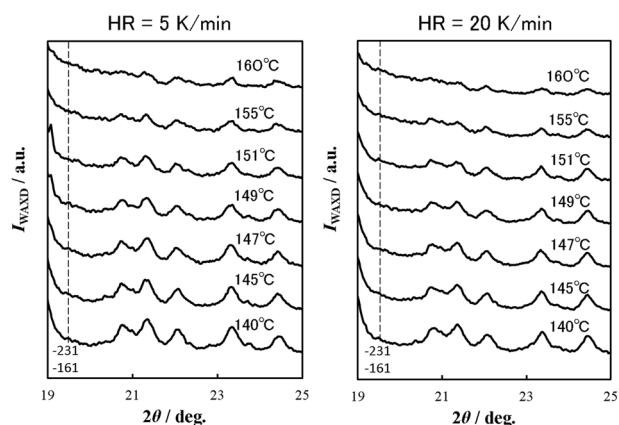


Fig. 2 Temperature dependencies of WAXD profiles (high-angle region) for HR = 5 and 20 K/min

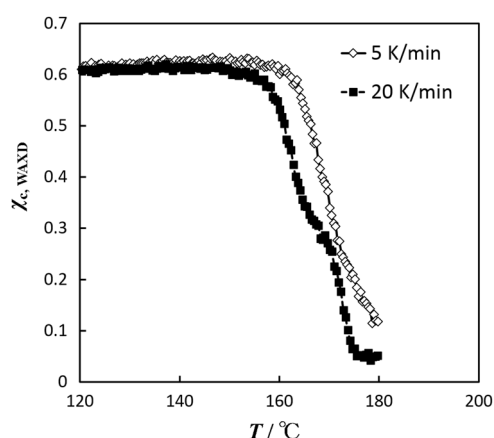


Fig. 3 Temperature dependencies of $\chi_{c,WAXD}$ for HR = 5 and 20 K/min

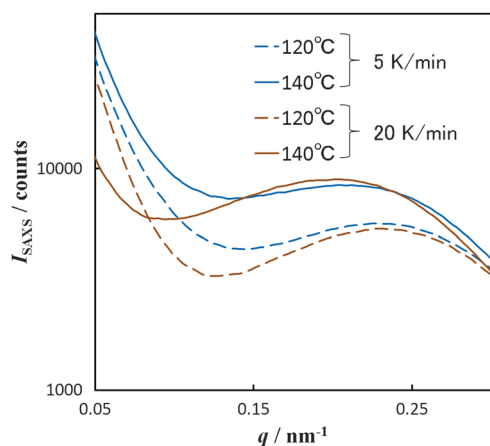


Fig. 4 Temperature dependencies of SAXS profiles for HR = 5 and 20 K/min

increasing temperatures at different HRs, the intensity of central diffuse scattering increased at 140 °C compared to 120 °C for a low HR of 5 K/min but decreased at 140 °C compared to 120 °C for the high HR of 20 K/min. Figure 5

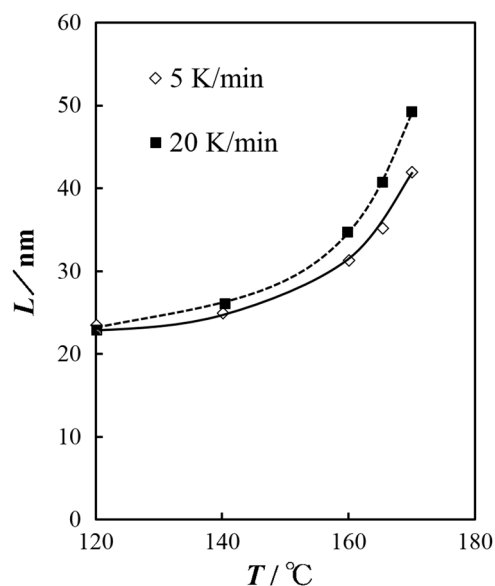


Fig. 5 Temperature dependencies of L for HR = 5 and 20 K/min

shows the temperature dependencies of L for HR = 5 and 20 K/min. L rapidly increased above 160 °C, and the degree of increase was slightly higher for a high HR of 20 K/min than for a low HR of 5 K/min.

Structure of samples heat-treated near their melting point for a short time

The heat treatment of the melt-crystallized sample was conducted under the following two conditions using the DSC.

Heat treatment at 160 °C for 4 min followed by cooling at a CR of 20 K/min (denoted as “160C4m”).

Heat treatment at 155 °C for 1 min and further at 160 °C for 3 min followed by cooling at a CR of 20 K/min (denoted as “155C1m-160C3m”).

A pretreatment at 155 °C for 1 min of 155C1m-160C3m was introduced because it is considered to correspond to heating at a low HR of 5 K/min. The total time of heat treatment was chosen as 4 min because the sample remains between 140 and 160 °C for 4 min during melting at an HR of 5 K/min in the experiment described in the section “Structural change during melting with different HRs”. The beginning and final temperatures were 30 °C. The HR between the start and treatment temperatures, as well as that between the treatment temperatures, was 200 K/min. It was confirmed that there was no temperature overshooting by monitoring the temperature of a sample during the heat treatments. The main heat treatment temperature was chosen as 160 °C for 3 min because it produced the highest crystallinity measured via the endothermic peak area of the DSC melting curve for a sample that was heat-treated at a single temperature. Also, 155 °C was chosen as a

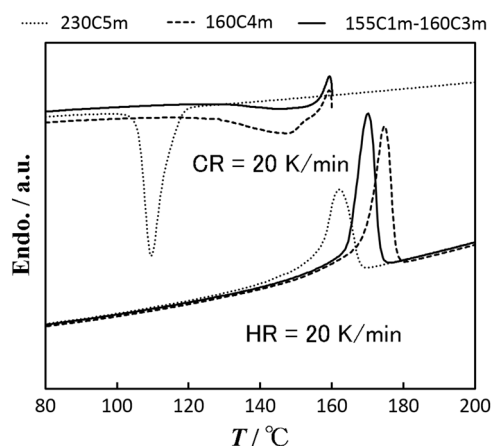


Fig. 6 DSC cooling profiles at CR = 20 K/min and subsequent melting profiles at HR = 20 K/min after melting at 230 °C for 5 min and after subsequent heat treatments by different conditions

pretreatment temperature for 1 min prior to the main heat treatment at 160 °C for 3 min because it produced the highest crystallinity measured via the endothermic peak area of the DSC melting curve for a sample that was heat-treated with the preheating process.

Figure 6 shows the DSC cooling profiles at CR = 20 K/min after melting at 230 °C for 5 min and after the subsequent heat treatments of 230C5m under the two different conditions. A sharp exothermic peak was observed at 109.5 °C after melting at 230 °C for 5 min, whereas relatively smaller and broader exothermic peaks were observed at 146–147 °C after the heat treatments. The exothermic peak of 160C4m was much larger than those of 155C1m-160C3m.

Figure 6 also shows melting profiles after cooling at a CR of 20 K/min for the melt-crystallized and the heat-treated samples. The peaks of the melting curves were 162.2 °C, 174.6 °C, and 170.3 °C for 230C5m, 160C4m, and 155C1m-160C3m, respectively. The melting peak of 155C1m-160C3m was sharper compared to that of 160C4m.

Figure 7 shows optical microscopy images for 230C5m, 160C4m, and 155C1m-160C3m. It is apparent that the spherulite morphology of 230C5m was maintained after the subsequent heat treatments. The heat-treated samples (160C4m and 155C1m-160C3m) showed more pronounced birefringence than the original melt-crystallized sample (230C5m).

Figure 8 shows the circle ring average of a 2D WAXD profile detected by IP for 230C5m, 160C4m, and 155C1m-160C3m. The 300 reflection of the β crystal was only observed for 230C5m around $2\theta = 16^\circ$. A subtle 117 reflection of the γ crystal was only observed for 160C4m around $2\theta = 20^\circ$. The values of $\chi_{c, WAXD}$ were 66%, 74%, and 75% for 230C5m, 160C4m, and 155C1m-160C3m, respectively. $\chi_{c, WAXD}$ increased drastically due to the heat treatments, and 155C1m-160C3m had slightly higher

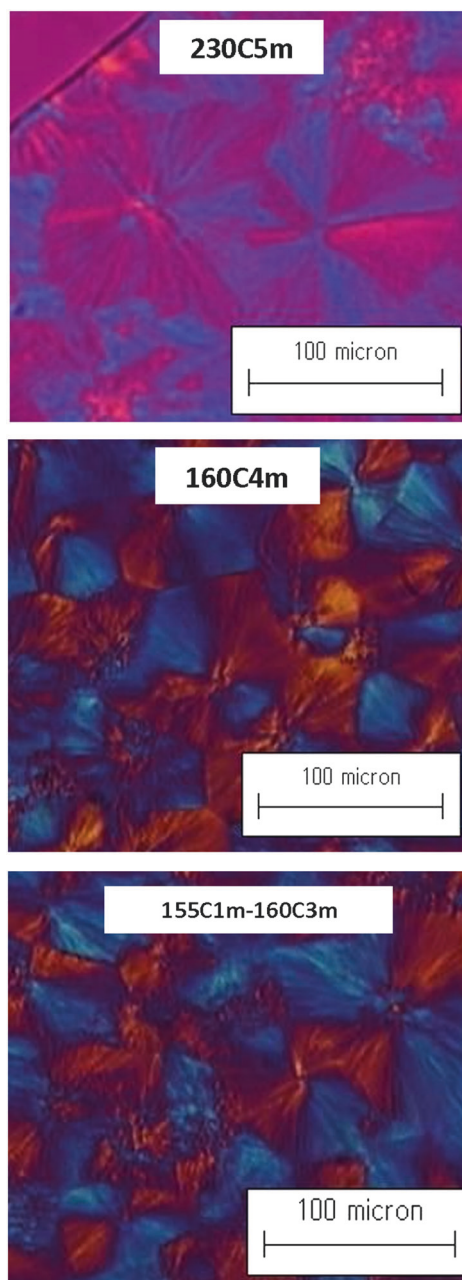


Fig. 7 Optical microscopy images for the sample that was crystallized from the melt by cooling at CR = 20 K/min and for samples subsequently heat-treated under different conditions

crystallinity than 160C4m. Figure 8 also shows the WAXD profile in the high-angle region. The measures of the ratio of the α_2 crystal (M_{α_2}) were 0%, 61%, and 41% for 230C5m, 160C4m, and 155C1m-160C3m, respectively. 160C4m had a much higher α_2 crystal content than 155C1m-160C3m.

Figure 9 shows the circle ring average of the 2D SAXS profile detected by IP for 230C5m, 160C4m, and 155C1m-160C3m. The peak position was drastically shifted to a lower angle for the heat-treated samples, suggesting an increase in the long period (L) for those

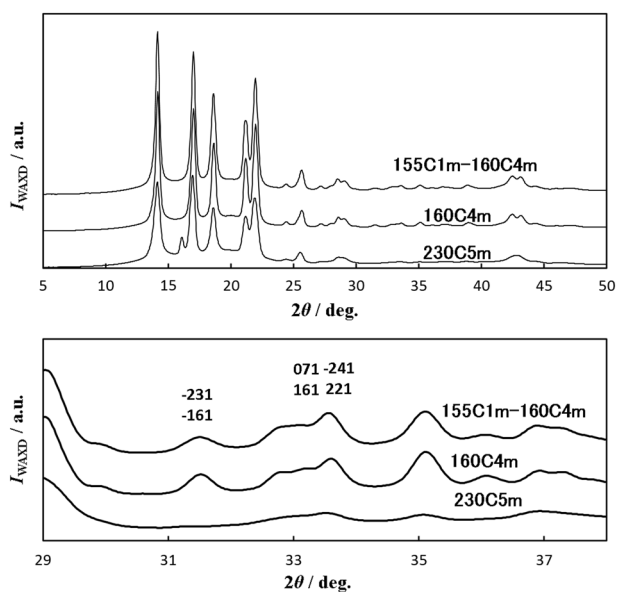


Fig. 8 Circle ring average of two-dimensional WAXD profiles for the sample that was crystallized from the melt by cooling at CR = 20 K/min and for samples subsequently heat-treated under different conditions (above) and profiles in the high-angle region (below)

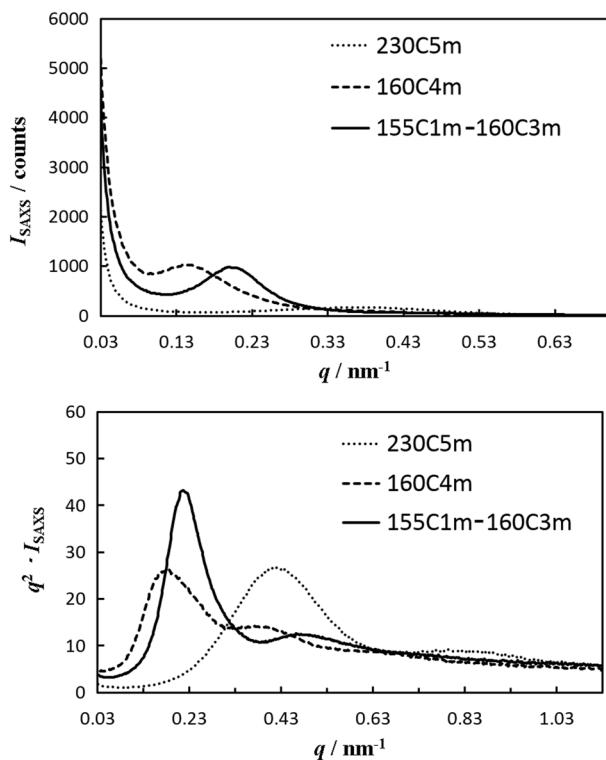


Fig. 9 Circle ring average of two-dimensional SAXS profiles (above) and profiles in the wider angle region after the Lorentz correction (below) for a sample that was crystallized from the melt by cooling at CR = 20 K/min and for samples subsequently heat-treated under different conditions

samples. The increase in L was larger for 160C4m than for 155C1m-160C3m. The intensity of central diffuse scattering also increased drastically for the heat-treated samples. The increase in the intensity of central diffuse scattering was larger for 160C4m than for 155C1m-160C3m. We also attempted an analysis of the central diffuse scattering using a Guinier plot [12], but no region that satisfied $q \ll 1/R_g$ was found, where R_g is the radius of gyration. Figure 9 also shows the Lorentz-corrected SAXS profiles for 230C5m, 160C4m, and 155C1m-160C3m. After the Lorentz correction, a second-order diffraction peak was observed for all samples. The L values were 14.9, 34.8, and 28.5 nm for 230C5m, 160C4m, and 155C1m-160C3m, respectively. L more than doubled due to the subsequent heat treatment at 160 °C for 4 min and nearly doubled due to the subsequent heat treatment at 155 °C for 1 min plus 160 °C for 3 min. The peak corresponding to the long period of 155C1m-160C3m was sharper than that of 160C4m.

Figure 10 shows transmission electron micrographs for 230C5m, 160C4m, and 155C1m-160C3m. An increase in lamellar thickness (l_c) was observed for the heat-treated samples. The average lamellar thicknesses ($\langle l_c \rangle$) obtained from the micrographs were 7.8, 11.2, and 9.9 nm for 230C5m, 160C4m, and 155C1m-160C3m, respectively. The regularity of lamellar stacking decreased due to the heat treatments. The increase in l_c and the decrease in the regularity of lamellar stacking were larger for 160C4m compared to 155C1m-160C3m. It should also be noted that lamellae of 160C4m were more discontinuous in the lateral direction, and as a result, their dimensions in the lateral direction were much shorter than those of 155C1m-160C3m.

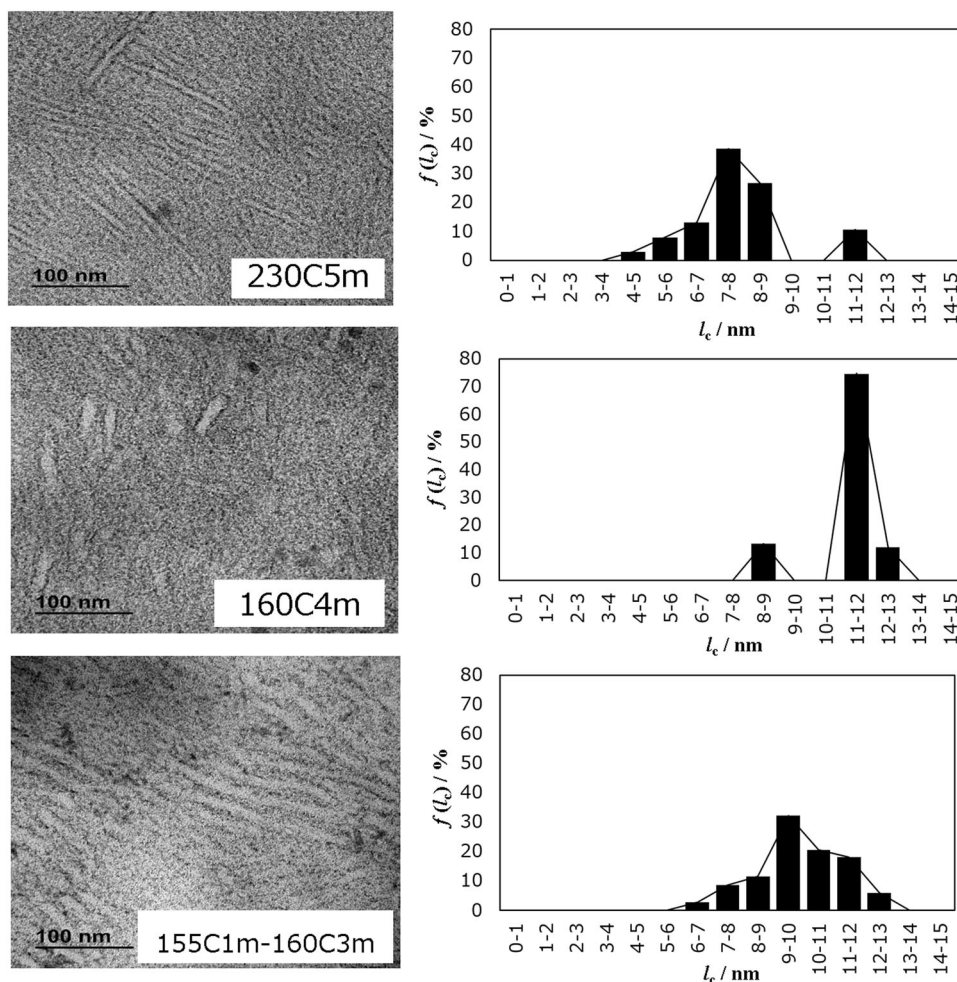
Table 1 summarizes the experimental results mentioned above.

Discussion

Structural and morphological changes commonly associated with melting and heat treatments

Melting at a low HR of 5 K/min and heat treatments near the melting point for a short time have many common features. During melt-crystallization via cooling at CR = 20 K/min to produce the initial sample (230C5m), an exothermic peak of crystallization was observed at 109.5 °C (Fig. 6). During such low-temperature crystallization, crystals with thin lamellar thicknesses (l_c) are generated [2]. When the thin lamellar crystal is heated by a low HR, the melting point increases due to the thickening of lamellar crystals [2]. Therefore, the higher melting peak of 168 °C

Fig. 10 Transmission electron micrographs and histograms of lamellar thickness (l_c) for a sample that was crystallized from the melt by cooling at CR = 20 K/min and for samples subsequently heat-treated under different conditions



observed during heating at a low HR of 5 K/min (Fig. 1) is considered to correspond to the melting of thick lamellar crystals that is generated by reorganization during heating. $\chi_{c, \text{WAXD}}$ was maintained in a higher temperature region at a lower HR of 5 K/min than at a higher HR of 20 K/min (Fig. 3), which supports the above hypothesis. The heat-treated samples (160C4m and 155C1m-160C3m) also showed a higher T_m of 174.6 and 170.3 °C (Fig. 6 and Table 1) and correspondingly larger average lamellar thicknesses ($\langle l_c \rangle$) of 11.2 and 9.9 nm (Fig. 10 and Table 1) than those (162.2 °C and 7.8 nm) of the starting sample (230C5m). The increases in l_c and T_m can therefore be understood as a function of lamellar thickening [13]. Experimental [14] and theoretical [15] studies on the mechanism of lamellar thickening at initial stages of crystallization have been reported for polyethylene. The values of long periods (L) were more than twice $\langle l_c \rangle$ for the heat-treated samples, which suggests that there are some crystalline portions between the lamellae considering the values of $\chi_{c, \text{WAXD}}$ associated with these samples. We did not clearly recognize these crystalline portions in our TEM observation, although there are some areas where another

Table 1 Summary of experimental data

	T_m (°C)	$\chi_{c, \text{WAXD}}$ (%)	$M_{\alpha 2}$ (%)	L (nm)	$\langle l_c \rangle$ (nm)
230C5m	162.2	66	0	14.9	7.8
160C4m	174.6	74	61	34.8	11.2
155C1m-160C3m	170.3	75	41	28.5	9.9

lamella seems to penetrate two thick lamellae in the heat-treated samples.

The increase in the intensity of central diffuse scattering of SAXS was also observed both during the melting process at a low HR of 5 K/min (Fig. 4) and for the samples that were heat-treated near their melting points for a short time (Fig. 9). The structural origin of central diffuse scattering is the existence of scattered components without positional correlation, and the profile depends on the size and shape of the scattered components [16]. The increase in diffuse scattering observed at the low HR of 5 K/min and the heat-treated samples is considered to be associated with crystals that were generated by lamellar thickening during heating.

A similar increase in central diffuse scattering of SAXS was also reported for the crystallization of polyethylene [17]. The TEM micrographs of the heat-treated samples showed irregularity of lamellar stacking, and the irregularity was enhanced for 160C4m, for which the holding time at a higher temperature (160 °C) was longer compared to 155C1m-160C3m. A similar increase in irregularity of lamellar stacking was also reported for the crystallization of polypropylene at high temperatures [18].

L rapidly increased above 160 °C and became more than 30 nm during melting both at an HR of 20 and 5 K/min (Fig. 5). Due to the heat treatments where the HR from 30 °C to the initial heat treatment temperatures was 200 K/min, L became 34.8 and 28.5 nm for 160C4m and 155C1m-160C3m, respectively, which means that L largely increased due to changing the heat treatment temperature from 155 °C to 160 °C in the first 1 min (Fig. 9; Table 1). These sharp increases in L are due to the melting of thin lamellar crystals that exist between thick lamellar crystals [19]. The increased L during the heat treatments due to the partial melting of the thin lamellae is considered to be maintained even after the heat treatment procedures including subsequent cooling are complete due to the aforementioned reorganization.

Features of the structural and morphological changes due to melting and heat treatments

The reflections of -161 and -231 , a measure of the $\alpha 2$ crystal, were not clear during melting at a low HR of 5 K/min (Fig. 2), which suggests that the reorganization during heating at a low HR of 5 K/min does not originate from recrystallization but from lamellar thickening of the $\alpha 1$ crystal. On the other hand, certain amounts of the $\alpha 2$ crystal ($M_{\alpha 2} = 61\%$ for 160C4m and $M_{\alpha 2} = 41\%$ for 155C1m-160C3m) were observed for the heat-treated samples (Fig. 8; Table 1). Two reasons can be considered for this difference. One is due to melting of the $\alpha 1$ crystal and recrystallization to an $\alpha 2$ crystal [20]. Another is due to the existence of a portion of the melt that could not crystallize during the heat treatments and rather crystallized during subsequent cooling. As shown in Fig. 6, an exothermic peak occurs near 146–147 °C, the temperature at which the $\alpha 2$ crystal is formed [3], in the DSC profiles during cooling after the heat treatments. This suggests that the heat-treated samples contain the portion of the $\alpha 2$ crystal that formed during cooling after the heat treatments. The area of the exothermic peak was much larger for 160C4m compared to 155C1m-160C3m, suggesting that a larger amount of melt that could not crystallize remained after the heat treatments. This could be one of the reasons why $M_{\alpha 2}$ is much larger in 160C4m than in 155C1m-160C3m. In contrast, as shown in Fig. 8 and Table 1, χ_c , χ_{WAXD} was even slightly higher for

155C1m-160C3m compared to 160C4m, suggesting that the lamellar thickening had a greater effect on the increase in crystallinity. The enhancement of crystallization by preheating at 155 °C is interpreted as support that lamellae with increased l_c during preheating acted as nuclei during crystallization at 160 °C [21].

Conclusion

Time-resolved X-ray measurements during melting and detailed structural and morphological analyses of heat-treated samples near their melting temperatures for a short time revealed the type of structural change for an iPP that was crystallized from the melt at a CR = 20 K/min. The observations performed by X-ray and TEM imaging suggest that the main mechanism of this reorganization is lamellar thickening of the $\alpha 1$ crystals and not melt-recrystallization. We also found that lamellar stacking was disordered in this reorganization process at high temperatures. The drastically increased L at the near-melting temperature was maintained after the heat treatments by the reorganization of thin lamellae, which partially melted during heating.

Acknowledgements In performing this research, Dr. Hiroyasu Masunaga and Dr. Taizo Kabe (Japan Synchrotron Radiation Research Institute), who are in charge of BL 03 XU (Frontier Soft Matter Beam Line), gave us great technical support. In addition, valuable advice was provided by Prof. Ken Kojio (Kyushu University) and Prof. Masatoshi Kitida (Tokyo Institute of Technology). We would like to express our gratitude to them.

Compliance with ethical standards

Conflict of interest There is no conflict of interest in relation to our present publication.

References

1. Toda A, Taguchi K, Sato K, Nozaki K, Maruyama M, Tagashira K, et al. Melting kinetics of *it*-polypropylene crystals over wide heating rates. *J Therm Anal Calorim*. 2013;113:1231–237.
2. Yamada K, Hikosaka M, Toda A, Yamasaki S, Tagashira K. Equilibrium melting temperature of isotactic polypropylene with high tacticity: 1. Determination by differential scanning calorimetry. *Macromolecules*. 2003;36:4790–801.
3. Sato K, Nozaki K, Toda A, Kajioka H, Tagashira K, Yamada K, et al. Structural formation of $\alpha 1$ phase and $\alpha 2$ phase of isotactic polypropylene: II. Structural change in temperature jump annealing. *Proc Polym Soc*. 2010;59:3PC041.
4. Hikosaka M, Seto T. The order of the molecular chains in isotactic polypropylene crystals. *Polym J*. 1973;5:111–27.
5. Japanese Patent Application Publication No. JP 2011-195830.
6. Asakawa H, Nishida K, Kanaya T, Tosaka M. Giant single crystal of isotactic polypropylene showing near-equilibrium melting temperature. *Polym J*. 2013;45:287–92.

7. Yamada K, Hikosaka M, Toda A, Yamasaki S, Tagashira K. Molecular weight dependence of equilibrium melting temperature and lamellar thickening of isotactic polypropylene with high tacticity. *J Macromol Sci B*. 2003;42:733–52.
8. Cheng SZD, Janimak JJ, Zhang A. Isotacticity effect on crystallization and melting in polypropylene fractions 1. Crystalline structures and thermodynamic property changes. *Polymers*. 1991;32:648–55.
9. Weidinger A, Hermans PH. On the determination of the crystalline fraction of isotactic polypropylene from X-Ray diffraction. *Macromol Chem Phys*. 1961;50:98–115.
10. Wilson AJC. *International tables for crystallography*. Dordrecht/Boston/London: Kluwer Academic Publishers; 1995. p. 518.
11. CSER F. About the Lorentz correction used in the interpretation of small angle X-Ray scattering data of semicrystalline polymers. *J Appl Polym Sci*. 2001;80:2300–8.
12. Roe RJ. *Methods of X-ray and neutron scattering in polymer science*. Oxford, UK: Oxford University Press Inc.; 2000. p. 167.
13. Fischer EW, Schmidt GF. On long periods of stretched polyethylene. *Angew Chem*. 1962;74:551–62.
14. Barham PJ, Keller A. The initial stages of crystallization of polyethylene from the melt. *J Polym Sci Polym Phys Ed*. 1989;27:1029–42.
15. Hikosaka M, Amano K, Rastogi S, Keller A. Lamellar thickening growth of an extended chain single crystal of polyethylene (II): ΔT dependence of lamellar thickening growth rate and comparison with lamellar thickening. *J Mater Sci*. 2000;35:5157–68.
16. Guinier A. *Theory and practice of X-ray crystallography*. Tokyo, Japan: Rigaku Denki KK; 1967. p. 546.
17. Dlugosz J, Fraser GV, Grubb D, Keller A, Odell JA, Goggin PL. Study of crystallization and isothermal thickening in polyethylene using SAXD, low frequency Raman spectroscopy and electron microscopy. *Polymers (Guildf)*. 1976;17:471–80.
18. Yamada K, Hikosaka M, Toda A, Yamasaki S, Tagashira K. Equilibrium melting temperature of isotactic polypropylene with high tacticity. 2. Determination by optical microscopy. *Macromolecules*. 2003;36:4802–12.
19. Maeda M, Miyasaka K, Ishikawa K. [35] Change in small angle X-ray diffraction of fiber due to temperature change. *Polym Chem*. 1969;26:241–8.
20. Maeda Y, Nozaki K, Fujikawa T, Toda A, Maruyama M, Tagashira K, et al. $\alpha 1 \rightarrow \alpha 2$ phase transition of isotactic polypropylene crystal—in situ observation of melting and recrystallization. *Proc Polym Soc*. 2013;62:1PC045.
21. Fillon B, Wittmann JC, Lotz B, Thierry A. Self-nucleation and recrystallization of isotactic polypropylene (α phase) investigated by differential scanning calorimetry. *J Polym Sci Polym Phys Ed*. 1993;31:1383–93.